Modifications of the Torque-Bias Profile for Improved Tracking of Beam-Waveguide Antennas

W. Gawronski,[1] J. J. Brandt,[2] H. G. Ahlstrom, Jr.,[1] and E. Maneri[3]

Gearboxes and gears are part of the DSN antenna drives. The drives show backlash at the gearboxes and at elevation bull gears due to a small gap between the gear teeth. Left uncorrected, backlash deteriorates the antenna pointing precision. Implementing two identical drives imposes two nonidentical torques and produces a torque difference (also known as torque bias or counter-torque) that eliminates backlash. The electronic circuit at the axis drive generates the torque-bias profile. The performance of the existing circuit is analyzed, and a modified circuit is designed that improves the antenna dynamics under external disturbances.

I. Introduction

Gearboxes and gears are components of the DSN antenna drives. A backlash phenomenon at the gearboxes and at bull gears is observed when one gear rotates through a small angle without causing a corresponding movement of the second gear. This eventually causes beating in the drives, gear wear, and deterioration of antenna tracking precision. In order to maintain antenna pointing precision, the backlash phenomenon is eliminated by implementing two drives with a specific torque difference between them. The torque difference is called a torque bias, or counter-torque. With a two-motor configuration, backlash clearance will occur at one drive while the other is still coupled. The antenna dynamics will be controlled by the latter drive. The effectiveness of the two-motor approach depends on the amount of torque bias applied at the drives, which depends on the antenna load. The torque bias should be large enough to lead the antenna through the gap for the maximal allowable torque load, but small enough that it will not cause excessive local stress, friction, or wear.

High and steady loads do not need a torque bias since the backlash is observed for low and reversing axis loads only. Time-varying loads, such as wind gusts, can produce high torques that become very low within a short period of time, causing a backlash gap when the torque-bias dynamics are too slow. Reversing loads were observed at the DSS-13 antenna site when wind gusting caused the drives to grind. Thus, the proper dynamics of the torque bias-shaping loop were derived in this article to assure antenna tracking precision.

---

[1] Communications Ground Systems Section.

[2] Student at the University of Washington, Seattle.

[3] Student at Montana State University, Bozeman.

II. Backlash and Its Prevention

Consider a simple gearbox with two gears rotating in opposite directions. Let β_1 and β_2 be the angles of rotation of the first and second gears, respectively; N be the gearbox ratio; and k be the gearbox stiffness (at the second gear). In this case, the relationship between the gearbox rotation and the torque, T, at the second gear is as follows:

$$T_f = \begin{cases} 0 & \text{for } |\Delta\beta| \le b \\ k(\Delta\beta - b) & \text{for } \Delta\beta > b \\ k(\Delta\beta + b) & \text{for } \Delta\beta < -b \end{cases} \tag{1}$$

where $\Delta\beta = \beta_2 - \beta_1/N$, and b is the size of the backlash gap measured at the second gear. The plot of the torque versus the angle difference, $\Delta\beta$, is shown in Fig. 1 for $b = 1$ deg and $k = 20$ Nm/deg.

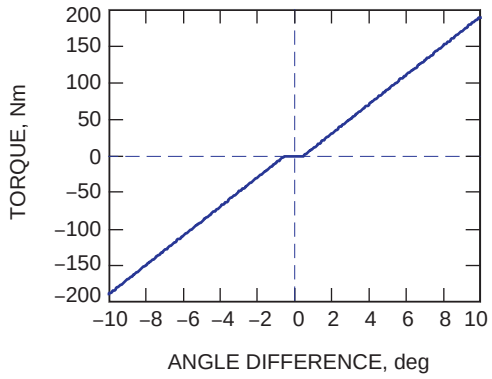

Fig. 1. The backlash function.

It is clear from the above equation that, if the angle difference of two gears is smaller than the backlash gap, b, there is a discontinuity in the gear motion, causing impacts of one gear tooth against the second gear tooth. Implementing two driving gears instead of a single one will minimize the impact of this discontinuity. In this approach, the driving torques, T_1 and T_2 of gears 1 and 2, are not identical but differ by the amount of ΔT. This difference is called the torque bias, or counter-torque.

When both gears are driven and the backlash occurs at the first gear, the torque at the second driving gear is nonzero (it differs by ΔT), and the antenna is driven smoothly. This principle of torque sharing is used in the beam-waveguide (BWG) antenna design.

The question remains of how large the torque bias must be to prevent backlash. If the stiffness of the gearbox is k, the torque bias, ΔT, should be greater than $2kb$. But, ΔT also depends on the load applied to the gears; no bias is required if the torque load is high ($T_1 \cong T_2 >> \Delta T$), because the angle difference is large and the backlash is not observed even when $\Delta T = 0$. Plots of the existing profile of motor torque versus axial load (as percentages of the maximal load) are shown in Fig. 2, for 10, 20, and 30 percent of the bias. The bias is largest for the low loads and phases out to zero for higher loads.

In the event of dynamic loading, such as wind gusts, the optimal magnitude of the torque bias is not obvious. During dynamic loading, the torque difference determined for the steady-state case may not be large enough to prevent the backlash, and assuming a higher counter-torque may lead to premature wear. Additionally, quickly varying loads with small, steady components may cause backlash in both gears simultaneously, despite the nonzero torque bias. Thus, the torque-bias time response also is an important design factor.

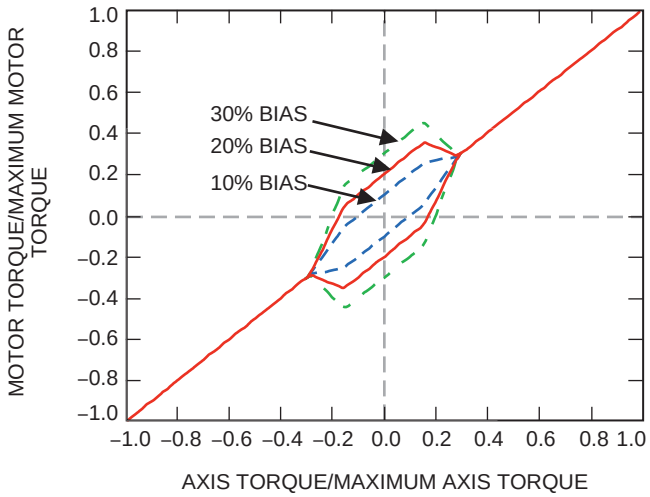

Fig. 2. Motor torque versus axial torque for a 10, 20, and 30 percent torque bias.

The purpose of torque-shaping analysis is to determine the value of the bias, the rate of phase out, and the dynamics of the counter-torque circuit.

III. Friction

Friction is a torque that always opposes motion. The friction torque, T_f, depends on the relative velocity, v, of the moving surfaces. After motion begins, friction is constant and referred to as the Coulomb friction torque, T_c. At zero relative speed, the friction torque, T_f, is equal and opposite to the applied torque, T_o, unless the applied torque is larger than the stiction torque, T_s. The latter is a torque at the moment of breakaway and is larger than the Coulomb torque. A diagram of the friction torque versus relative velocity is shown in Fig. 3. Denote $v_t > 0$, a velocity threshold, which is a small positive number; then the friction torque is

$$T_f = \begin{cases} -T_c \ \mathrm{sign}(v) & \text{for } |v| > v_t \\ -\min\left(|T_o|, T_s\right) \ \mathrm{sign}(T_o) & \text{for } |v| \le v_t \end{cases} \tag{2}$$

where T_o denotes the total applied torque, and $y = \mathrm{sign}(x)$ is a sign function: $y = 1$ for $x > 0$, $y = -1$ for $x < 0$, and $y = 0$ for $x = 0$. This equation states that, if the surfaces in contact develop measurable relative velocity, such that $v > v_t$, the friction torque is constant and directed opposite to the relative

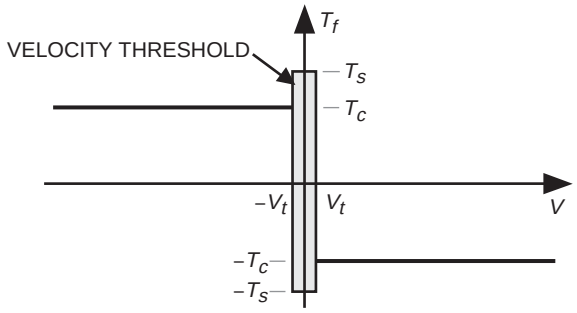

Fig. 3. Friction torque versus relative velocity.

speed. And, if the relative velocity is small, within the threshold ($v \leq v_t$), the friction torque does not exceed the stiction torque or the applied torque and is directed opposite to the applied torque. The velocity threshold, v_t, is included for numerical purposes since the zero state does not exist; thus, $v(i)$ is assumed to be zero if its absolute value is less than v_t.

In order to determine the friction torque, T_f, one must have the Coulomb friction torque, T_c; the stiction (breakaway) torque, T_s; the applied torque, T_o; and the wheel rate, v. The Coulomb friction torque is proportional to the normal force at the surface, F:

$$T_c = \mu r F \tag{3}$$

where r is the wheel radius and μ is the friction coefficient. For hard steel, $\mu = 0.0012 - 0.002$. The stiction (breakaway) torque, T_s, is most often assumed to be slightly higher than the Coulomb friction:

$$\left.\begin{array}{l} T_s = \alpha T_c \\ \\ \alpha = 1.2 - 1.3 \end{array}\right\} \tag{4}$$

The total applied torque, T_o, is determined as follows. Let the discrete state-space equation of the open-loop antenna be

$$x(i+1) = Ax(i) + B_u\ u(i) + B_f\ T_f(i) \tag{5a}$$

$$v(i) = Cx(i) \tag{5b}$$

where v is the antenna angular rate, T_f is the friction torque (either in azimuth or in elevation), and $(A, [B_u, B_f], C)$ is the state-space representation of the open-loop antenna. For the case of the antenna velocity within the threshold ($|v| \leq v_t$), we assume $v = 0$. Left multiplying Eq. (5a) by C, one obtains

$$v(i+1) = Cx(i+1) = CAx(i) + CB_u u(i) + CB_f T_f(i) \tag{6}$$

But, $v(i+1) = 0$; thus,

$$T_f(i) = -\frac{C}{CB_f}\left(Ax(i) + B_u u(i)\right) \tag{7}$$

and the applied torque, T_o, is opposite to the torque, T_f, i.e.,

$$T_o(i) = \frac{C}{CB_f}\left(Ax(i) + B_u u(i)\right) \tag{8}$$

IV. The Rate-Loop Model With Friction and Backlash

The motions of the antenna in the elevation and azimuth axes are uncoupled; therefore, they are analyzed independently. The Simulink model of the elevation-rate loop system is shown in Fig. 4 (Figs. 5 through 7 are also Simulink diagrams). The model contains the antenna structure with an elevation-rate input. The outputs are elevation encoder, elevation rate, elevation pinion rate, and elevation and cross-elevation pointing errors. The antenna-structure model is obtained from the DSS-13 finite-element model, as described in [1,2]. The elevation-drive model, which consists of the elevation-rate input, elevation pinion-rate inputs, and elevation-torque output, is shown in Fig. 5.

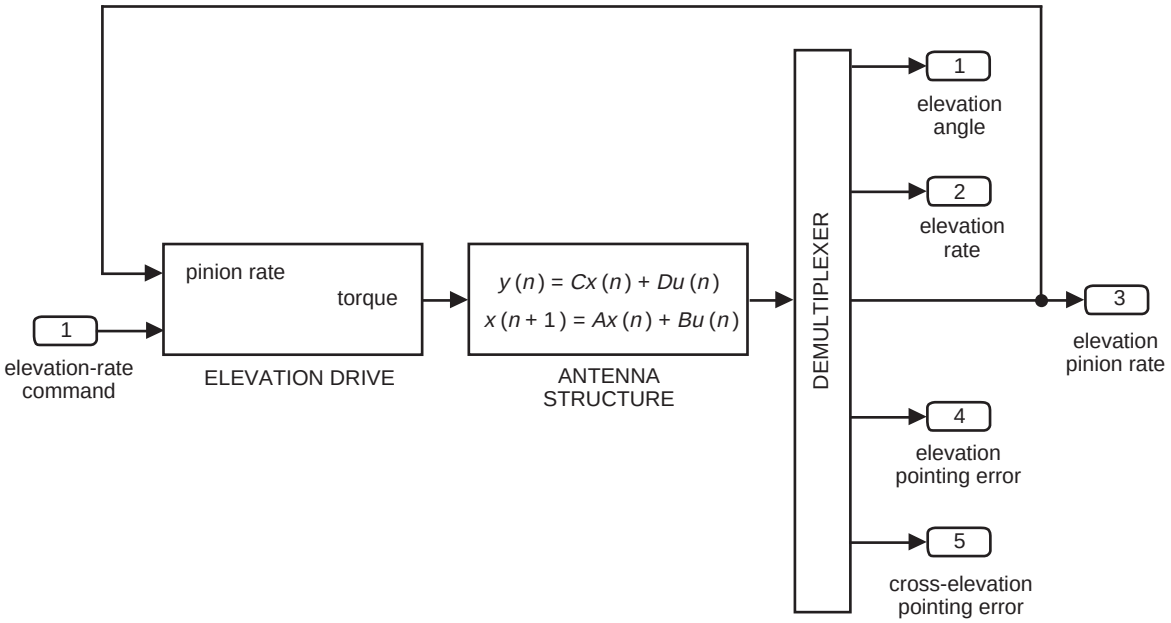

Fig. 4. The elevation-rate loop system.

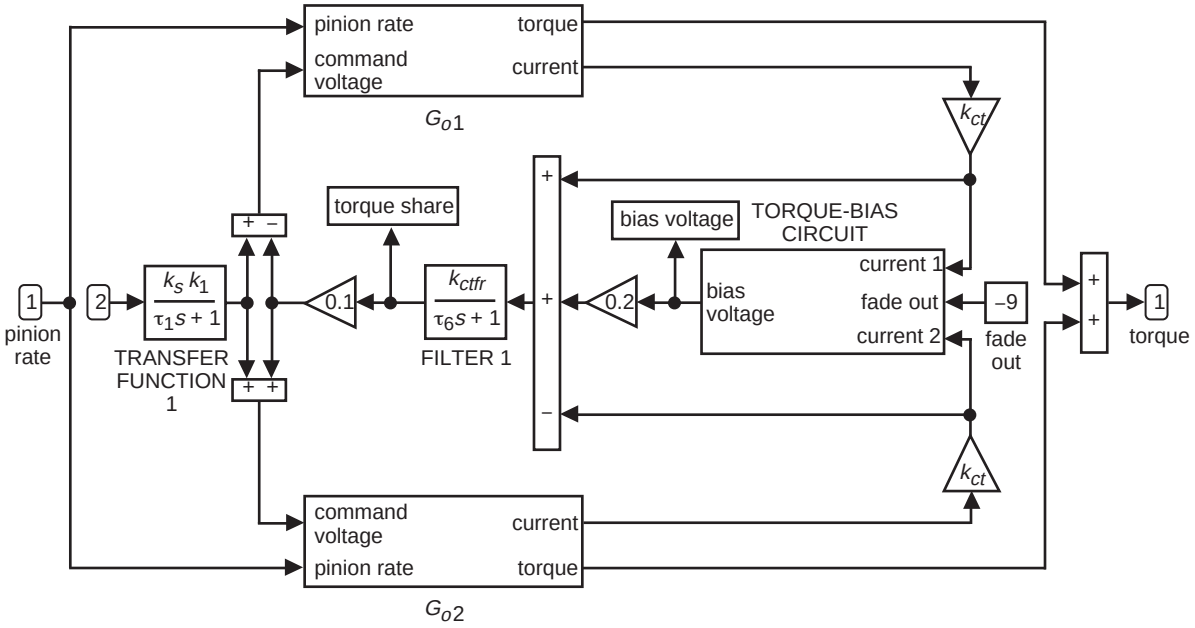

Fig. 5. The elevation drive.

The drive consists of two motors (with gearboxes), denoted G_o, and the torque-share circuit. Notation here is consistent with that of [1,2]. The block diagram of the subsystem, G_o, is shown in Fig. 6. It consists of two amplifiers, a motor armature, and a gearbox. The amplifiers and the motor armature are the same as those described in [1,2]. However, the gearbox model differs from the linear one in that it includes the nonlinear friction and backlash models (see Fig. 7). The friction torque in this model depends on the motor torque and the motor speed, as described earlier in Eq. (2). In the backlash model, the torque depends on the difference between the motor and the pinion angle, as in Eq. (1). The torque-share circuit, shown in Fig. 5, is described later in this article.

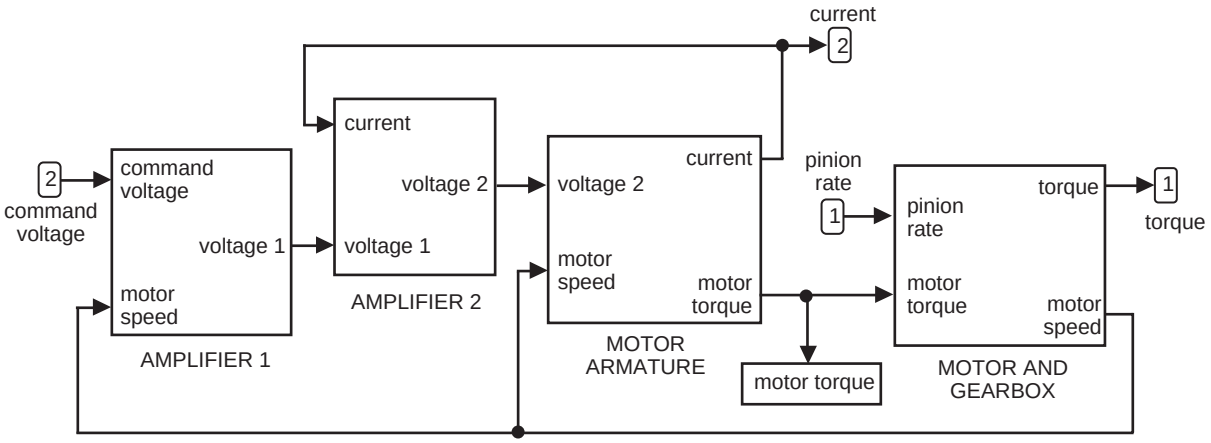

Fig. 6. The motor, gearbox, and amplifier (system G_o).

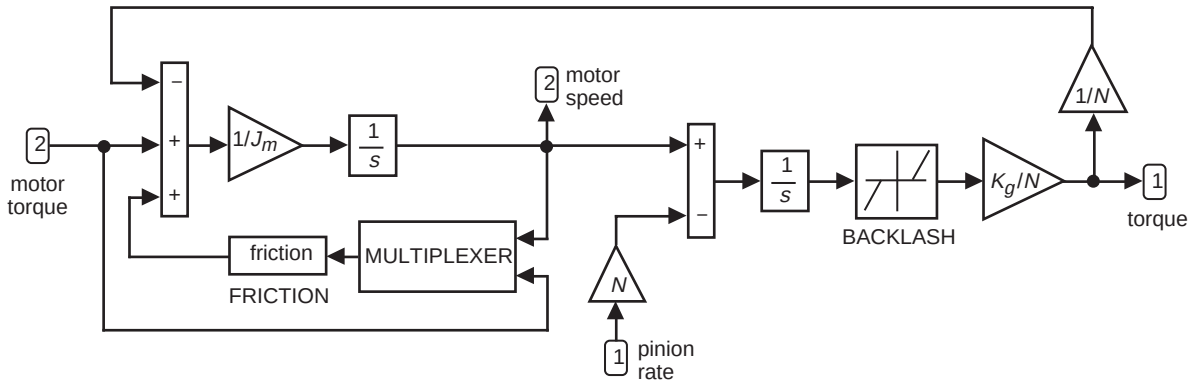

Fig. 7. The motor mechanical properties and gearbox.

The accuracy of the rate-loop model was verified experimentally. Open-loop tests were conducted at the DSS-26 antenna to compare the measured antenna dynamics with the simulated dynamics of the model, which includes backlash and friction. The test data were used to determine the amount of friction and the backlash angle. The rate-loop experiments were conducted by inserting the square-wave input of period 6.3 s and of amplitude 0.013 deg/s (this antenna rate corresponds to the tachometer rate of 193 deg/s). Two tests were conducted: one with zero torque bias and another with a torque bias of 15 percent of the maximal motor torque (the maximal torque is 308 kGm; thus, torque bias is 46 kGm).

For brevity of presentation, we consider the elevation axis only. For zero torque bias, the measured and simulated tachometer rates are shown in Figs.8(a) and 8(b), the measured and simulated motor currents are shown in Figs. 9(a) and 9(b), and the measured and simulated encoder readings in Figs. 10(a) and 10(b). These plots show satisfactory coincidence between the field data and simulation results.

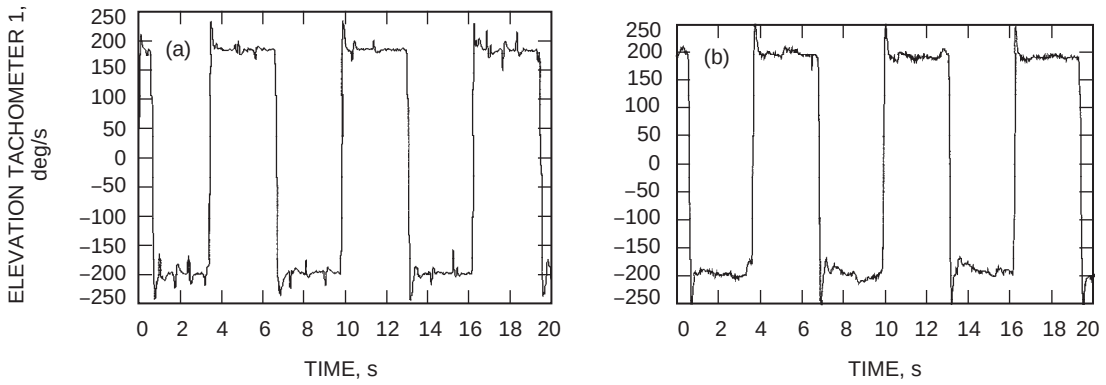

Fig. 8. Tachometer rates for zero torque bias: (a) measured and (b) simulated.

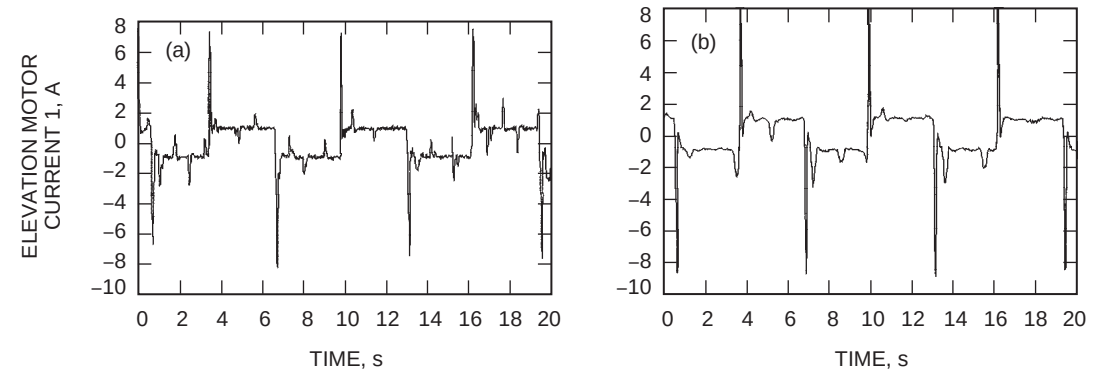

Fig. 9. Motor currents for zero torque bias: (a) measured and (b) simulated.

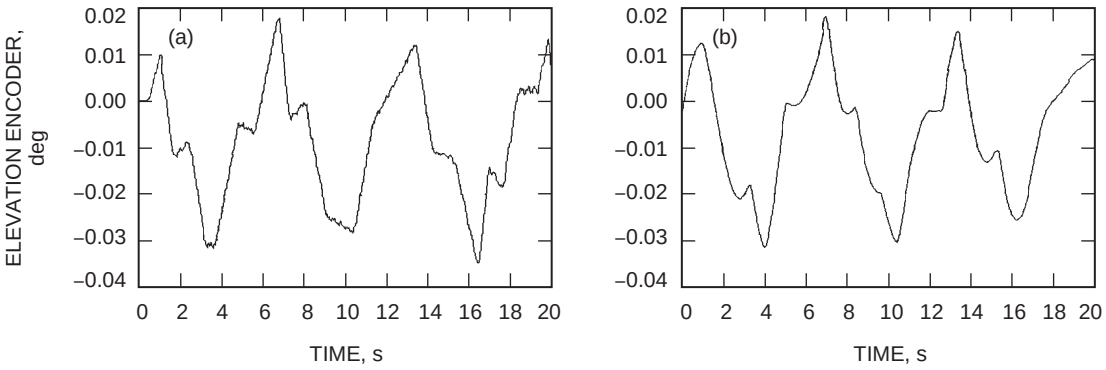

Fig. 10. Encoder readings for zero torque bias: (a) measured and (b) simulated.

In particular, the measured motor currents, which are proportional to the motor torque, allowed for the determination of the frictional torques. The constant part of the current in Fig. 9(a) is 1 A. It corresponds to the constant rate of the antenna movement, where no inertia forces are present, and the motor effort is totally dedicated to overcoming the friction forces. The 1-A current corresponds to the 61-kGm motor torque, or 9.1×10^5 kGm axis torque, which is the amount of the friction torque.

For the 15 percent torque bias, the plots of measured and simulated tachometer rates, motor currents, and encoder readings are given in Figs. 11(a) and 11(b) through 13(a) and 13(b), respectively. This situation is different from the zero-torque-bias case in that the encoder and tachometers show less chaotic movement of the antenna and the motor-torque plots indicate the presence of the torque bias, since their mean values are nonzero and have opposite signs.

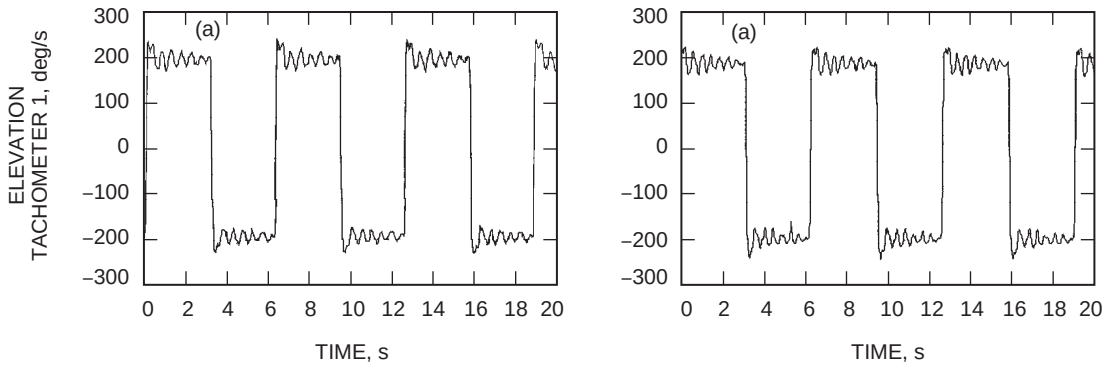

Fig. 11. Tachometer rates for 15 percent torque bias: (a) measured and (b) simulated.

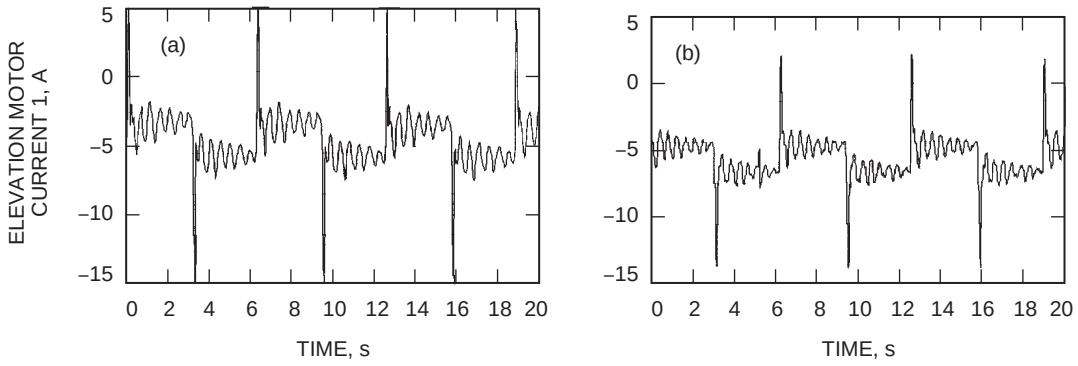

Fig. 12. Motor currents for 15 percent torque bias: (a) measured and (b) simulated.

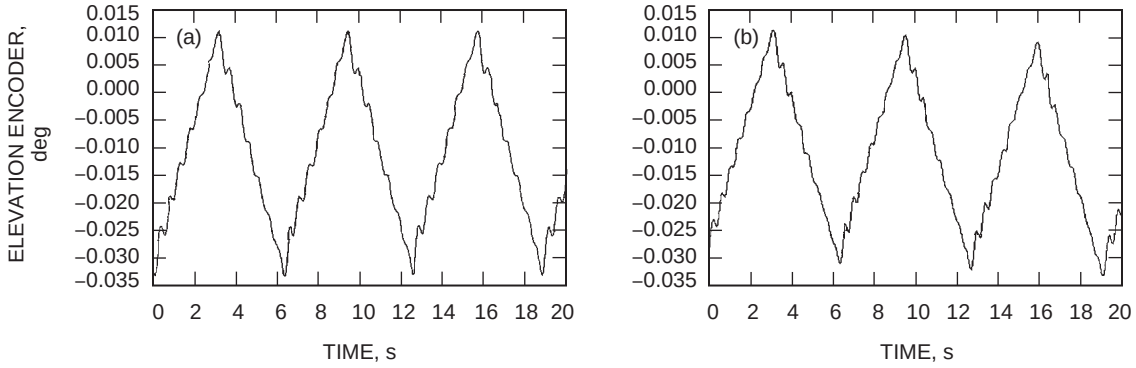

Fig. 13. Encoder readings for 15 percent torque bias: (a) measured and (b) simulated.

V. Modifications of the Bias Profile

The torque-share circuit is shown in Fig. 14. Its purpose is to determine the torque bias that is appropriate for the antenna load. Thus, the load in the form of motor current, i (transformed subsequently into voltage), is the circuit input. The fade-out voltage, f_o, is the additional voltage input that shapes the torque bias. The circuit output is the torque bias, v_b (given in volts). The relationship between the current, i (which is the sum of currents i_1 and i_2), and the bias voltage, v_b, follows from the block diagram in Fig. 14:

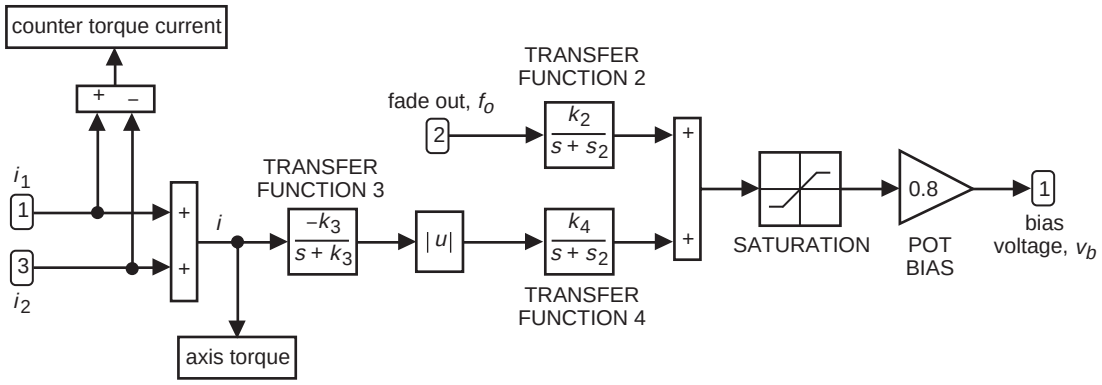

Fig. 14. The torque-share circuit.

$$v_b = k_p \; sat\left(G_2 f_o + G_4 \left|G_3 i\right|\right) \tag{9}$$

where G_2, G_3, and G_4 are transfer functions 2, 3, and 4, respectively, and k_p is the bias pot ($k_p = 0.8$). The parameters of the above transfer functions and Filter 1 for Fig. 5 are given in Table 1.

The saturation function, *sat*, is defined as follows:

$$sat(v) = \begin{cases} v_u & \text{if } v > v_u \\ v_l & \text{if } v < v_l \\ v & \text{elsewhere} \end{cases} \tag{10}$$

where the upper and lower limits of saturation are $v_u = 13\ V$ and $v_l = 0\ V$.

Note from the diagram in Fig. 14 that the transfer functions G_2 and G_4 are proportional; that is,

$$G_4 = k_2 G_2 \tag{11}$$

where $k_2 = 2.6$. Introducing Eq. (11) to Eq. (9), one obtains

Table 1. Filter and transfer function parameters.

Name	Parameter	Old value	New value
Filter 1	k_{ctfr}	4.54	66.67
	τ_6	1.369 s	8.889 s
Transfer function 1	k_s	0.8	0.8
	k_1	716.197 Vs/rad	716.197 Vs/rad
	τ_1	6.37×10^{-3} s	6.37×10^{-3} s
Transfer function 2	k_2	$-3.502\ s^{-1}$	$-2.114\ s^{-1}$
	s_2	$1.093\ s^{-1}$	$0.8895\ s^{-1}$
Transfer function 3	k_3	$2\ s^{-1}$	$3.831\ s^{-1}$
Transfer function 4	k_4	$2.8 \times k_2\ s^{-1}$	$1.617 \times k_2\ s^{-1}$

$$v_b = k_p \; sat\,(G_2(f_o + k_2\,|G_3 i|)) \tag{12}$$

The steady-state torque profile is obtained by replacing G_2 and G_3 with the corresponding DC gains, which are

$$G_3(0) = -1 \tag{13a}$$

and

$$g_2 = G_2(0) = -3.20 \tag{13b}$$

Thus, for the steady state, the bias voltage equation, Eq. (12), becomes the following:

$$v_b = k_p \; sat\,(g_2(f_o + k_2\,|i|)) \tag{14}$$

The plot of v_b versus i (proportional to the axis torque) for $k_p = 0.7$, $g_2 = -3.20$, $f_o = -9$ V, and $k_2 = 2.6$ (as implemented at DSS 13) is shown in Fig. 15(a) as a solid line. The bias can be shaped in three ways:

(1) By extending the constant value of the bias

(2) By changing the constant value of the bias

(3) By changing the slope of the bias

From Eq. (14), it follows that the first modification (the extension of the constant value of the bias) is obtained by changing the value of the fade-out voltage, f_o. The bias profile for the three different fade-out voltages is shown in Fig. 15(a), where the dashed line is for the fade-out voltage of -7 V, the solid line is for the fade-out voltage of -9 V, and the dashed–dotted line is for the fade-out voltage of -11 V. The higher (in absolute value) the voltage, the wider is the constant value of the bias.

By inspection of Eq. (14), one finds that the second modification (varying the constant value of torque bias) is obtained by varying the bias pot, k_p. The plots of bias voltage versus counter-torque current for bias pots of 0.3 (dashed–dotted line), 0.5 (dashed line), and 0.7 (solid line) are shown in Fig. 15(b). The plot shows that a larger bias pot results in a larger bias voltage. The slope is changed by varying the gain, g_2, of transfer function G_2. This is illustrated in Fig. 15(c) with three cases of gain scaling: the nominal gain, $g_2 = -3.20$ (solid line), the two-fold increased gain, $g_2 = -6.40$ (dashed line), and the reduced gain, $g_2 = -2.24$ (dashed–dotted line). The plots show that smaller gains result in smaller slopes. Finally, from Eq. (14), it follows that bias voltage depends on the gain k_2. This relationship is shown in Fig. 15(d), where the slope and horizontal extension of the bias are varied simultaneously after modifying k_2.

To prevent backlash in extreme dynamic loads, a flatter bias voltage is preferred, so gains g_2 and k_2 were modified according to the above relationships. The solid line in Fig. 16 shows the bias voltage profile for $g_2 = -2.38$ and $k_2 = 1.617$. This slope is smaller, as compared with the nominal, dashed line. The resulting profile (as a percentage of the maximal torque) is shown in Fig. 17 for 10, 20, and 30 percent of the bias. Compare this profile with that of the existing torque bias (Fig. 2) and note the sharp decline for the existing configuration as compared with the mild slopes of the modified design.

The performances of the old and new models have been verified analytically and in field testing of the rate-loop model. The bias voltage was chosen as an indicator of the quality of design. For best

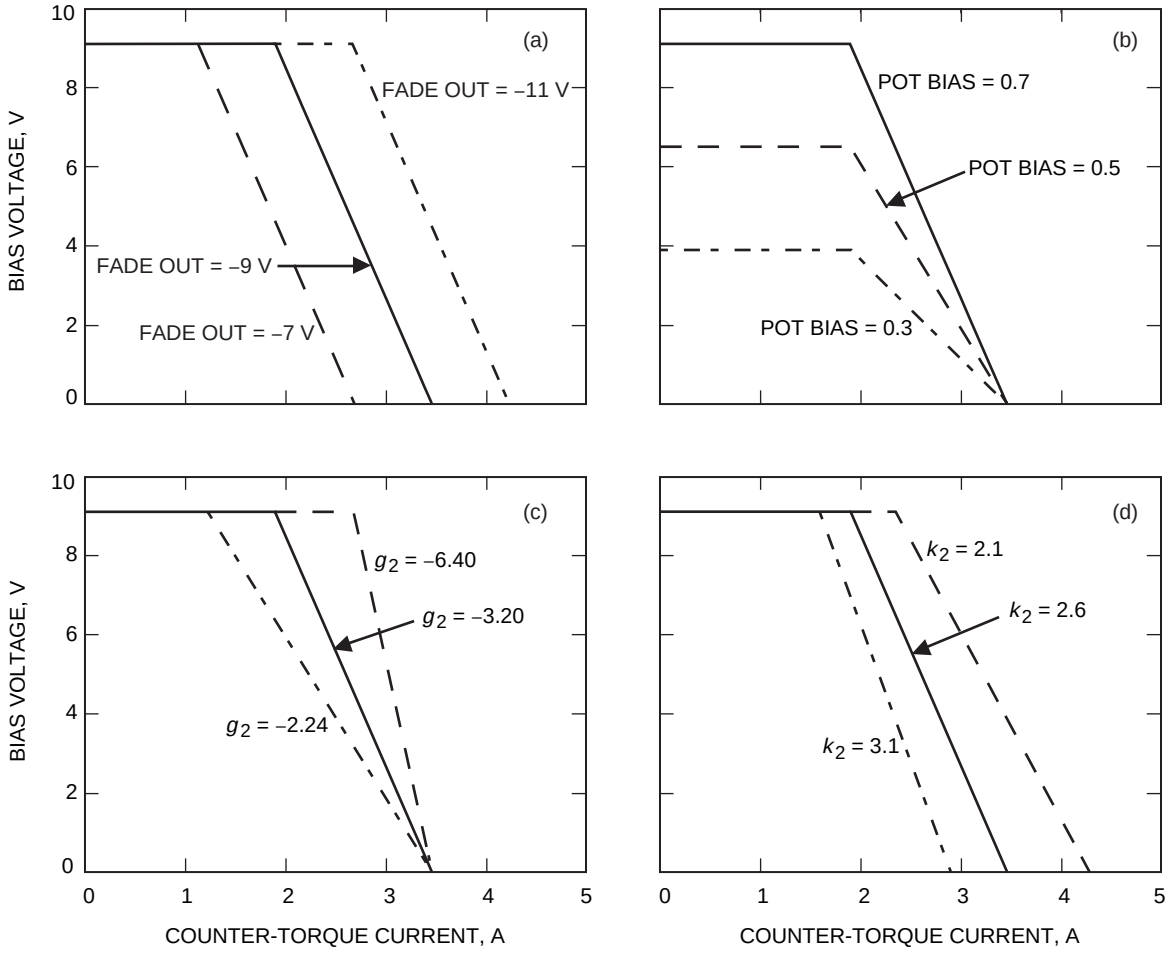

Fig. 15. Bias voltage versus axis torque for (a) fade-out voltages of –7, –9, and –11 V, (b) bias pots of 0.3, 0.5, and 0.7, (c) g_2, DC gain, nominal of –3.20, two-fold increased gain of –6.40, and reduced gain of –2.24 and (d) k_2 gains of 2.1, 2.6, and 3.1.

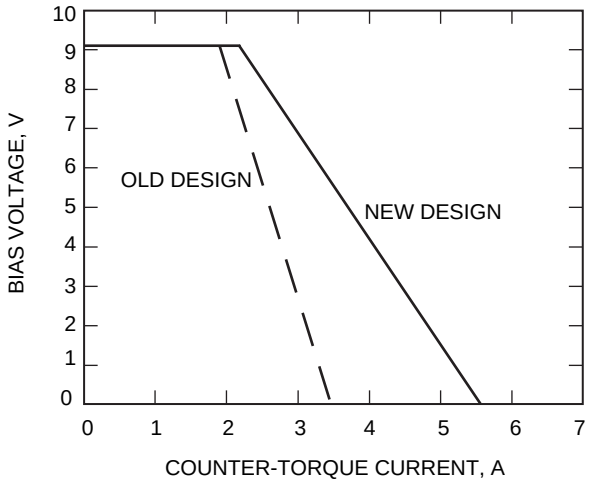

Fig. 16. Bias voltage versus axis torque for g_2 = –2.38 and k_2 = 1.617 (solid line) and for the existing gains (dashed line).

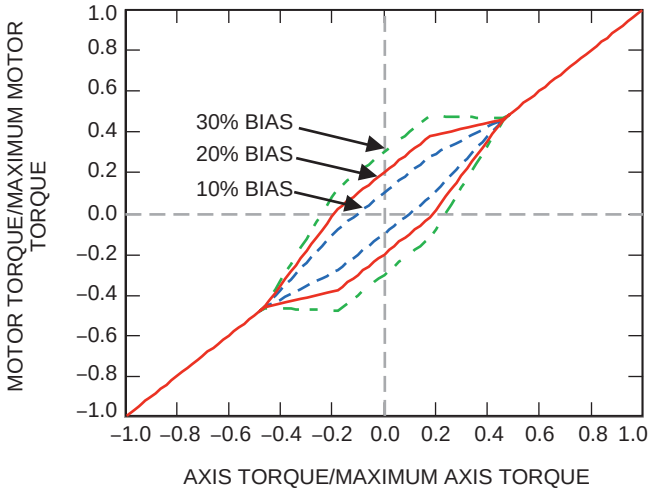

Fig. 17. Modified profile of motor torque versus axial torque for 10, 20, and 30 percent torque biases.

design results, the bias should remain at the maximum value. In an acceptable design, the bias always would be nonzero; if the bias remains at zero even for a small period of time, the backlash is observed and the design has not achieved its goals. The differences between these two designs can be exposed during high loads that vary abruptly. Therefore, a saw-tooth wave was chosen as a test signal to be applied at the antenna-rate loop input, with amplitude of 0.685 deg/s (85 percent of the maximal rate) and period of 5 s (see Fig. 18). The bias voltage of the old design with a saw-tooth input is shown in Fig. 19: the solid line as measured at DSS 26 and the dashed line as simulated using an analytical model. Both plots show a bias voltage that varies extensively and remains at zero for significant periods. The maximal bias is 11.2 V (field data) and 10.4 V (analysis), which are 86 and 80 percent of the maximal bias, respectively. The test results for the new design are shown in Fig. 20: the solid line for the field data and the dashed line for the simulations. Both show nonzero bias that varies from 8.0 to 11.4 V (field data) and from 7.2 to 11.6 V (analysis). This translates into 62 to 87 percent of maximal bias (field data) and into 56 to 88 percent of maximal bias (analysis). Data show that the bias-torque performance has significantly improved.

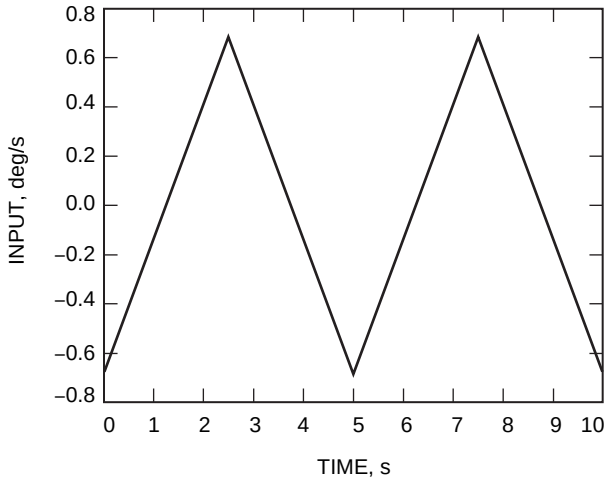

Fig. 18. The test signal.

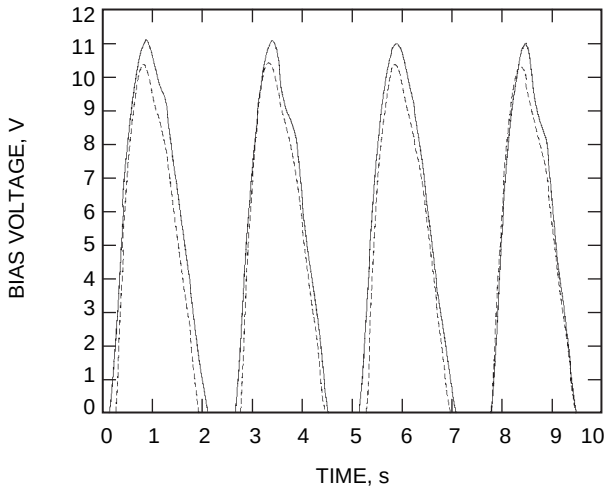

Fig. 19. Bias voltage under test signal for the old circuit design: from field tests (solid line) and from analysis (dashed line).

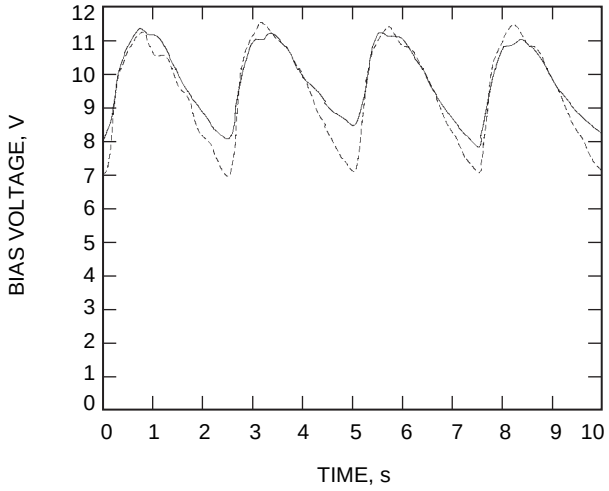

Fig. 20. Bias voltage under the test signal for the new circuit design: from field tests (solid line) and from analysis (dashed line).

VI. Improvements of the Bias-Torque Dynamics

The filter marked Filter 1 in the drive block diagram in Fig. 5 is responsible for the torque-bias dynamics. Its transfer function is as follows:

$$F_1 = \frac{k_{ctfr}}{1 + \tau_6 s} \tag{15}$$

with gain $k_{ctfr} = 3.31$ and time constant $\tau_6 = 0.73$ s. These filter constants are taken from the current design.

Denote i_1 and i_2 the currents of motor 1 and motor 2, respectively. The torque bias is proportional to their difference: $\Delta i = i_2 - i_1$. A simulated experiment in which a zero rate command was applied

recorded the relative torque bias: $(\Delta i/i_{\max}) \times 100$ percent. The initial torque bias was set to 0, and in the first period of antenna response that torque bias was raised to its nominal value (22 percent). The response is illustrated in Figs. 21(a) through 21 (e) with the (nominal) time constant of $\tau_6 = 0.73$ s and variable gains, k_{ctfr}, of 3.31, 33.14, 48.67, 69.60, and 106.03. The figures show that overshoot in the initial design is significant and that settling time is over 2 s. With an increased gain, the overshoot and settling time decrease. But too high of a gain ($k_{ctfr} > 146$) causes the system to go unstable (also confirmed in the field).

Next, the counter-torque dynamics were simulated with a nominal gain $k_{ctfr} = 3.31$ and variable time constant τ_6. The results are shown in Figs. 22(a) through 22(e) for τ_6 of 0.73, 0.20, 0.1125, 0.073, and 0.050 s, respectively. Again, the large initial overshoot decreased with decreasing τ_6, but, surprisingly, the settling time increased after an initial decrease.

After examining the impact of Filter-1 time constant and gain on counter-torque dynamics, $\tau_6 = 0.1125$ s, as in Fig. 22(c), and $k_{ctfr} = 48.67$, as in Fig. 21(c), were chosen for the new time constant and gain. Counter-torque dynamics resulting from the above parameters are shown in Fig. 23, where overshoot (0 percent) and settling time (0.8 s) have improved significantly.

VII. Conclusions

The 34-m BWG antenna backlash and friction were measured, modeled, and simulated. The torque-shaping circuit was analyzed, and a new bias-torque profile was developed. The new profile has flatter slopes, allowing for milder torque-bias variations regardless of load. The torque-bias dynamics are shaped with Filter 1 of the drive system. The existing filter parameters cause large torque-bias overshoot (80 percent) and settling time (2.4 s). The new filter causes no overshoot and a settling time of just 0.8 s. This torque-shaping circuit and filter were tested in the field, confirming the improved antenna performance.

References

[1] W. Gawronski and J. Mellstrom, "Modeling and Simulations of the DSS 13 Antenna Control System," *The Telecommunications and Data Acquisition Progress Report 42-106, April–June 1991*, Jet Propulsion Laboratory, Pasadena, California, pp. 205–248, August 15, 1991.
http://tmo.jpl.nasa.gov/tmo/progress_report/42-106/106R.PDF

[2] W. Gawronski, and J. A. Mellstrom, "Control and Dynamics of the Deep Space Network Antennas," chapter in *Control and Dynamic Systems*, C. T. Leondes, ed., vol. 63, San Diego, California: Academic Press, 1994.

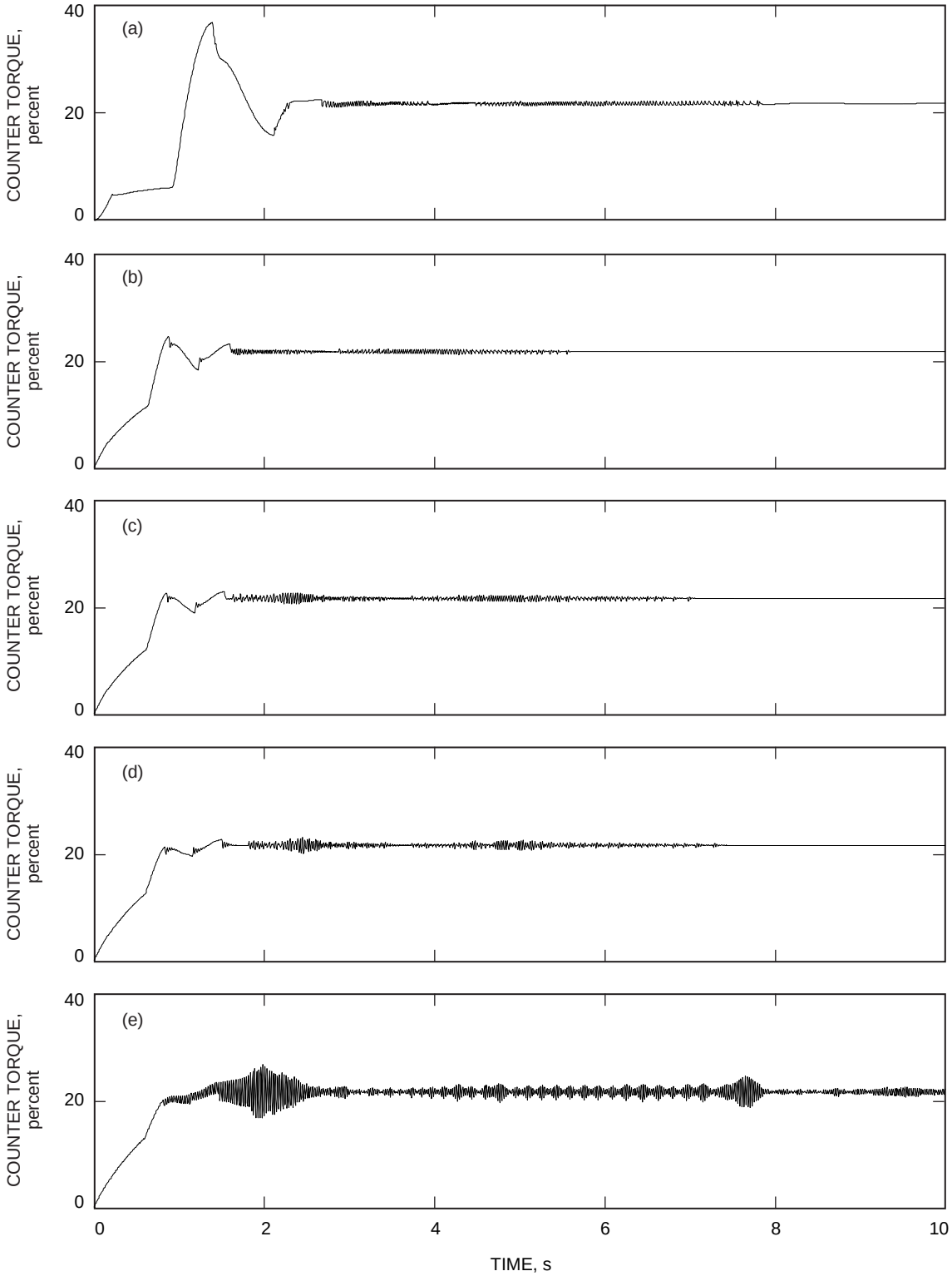

Fig. 21. Counter-torque dynamics for τ_6 = 0.73 s and for k_{ctfr} of (a) 3.31, (b) 33.14, (c) 48.67, (d) 69.60, and (e) 106.03.

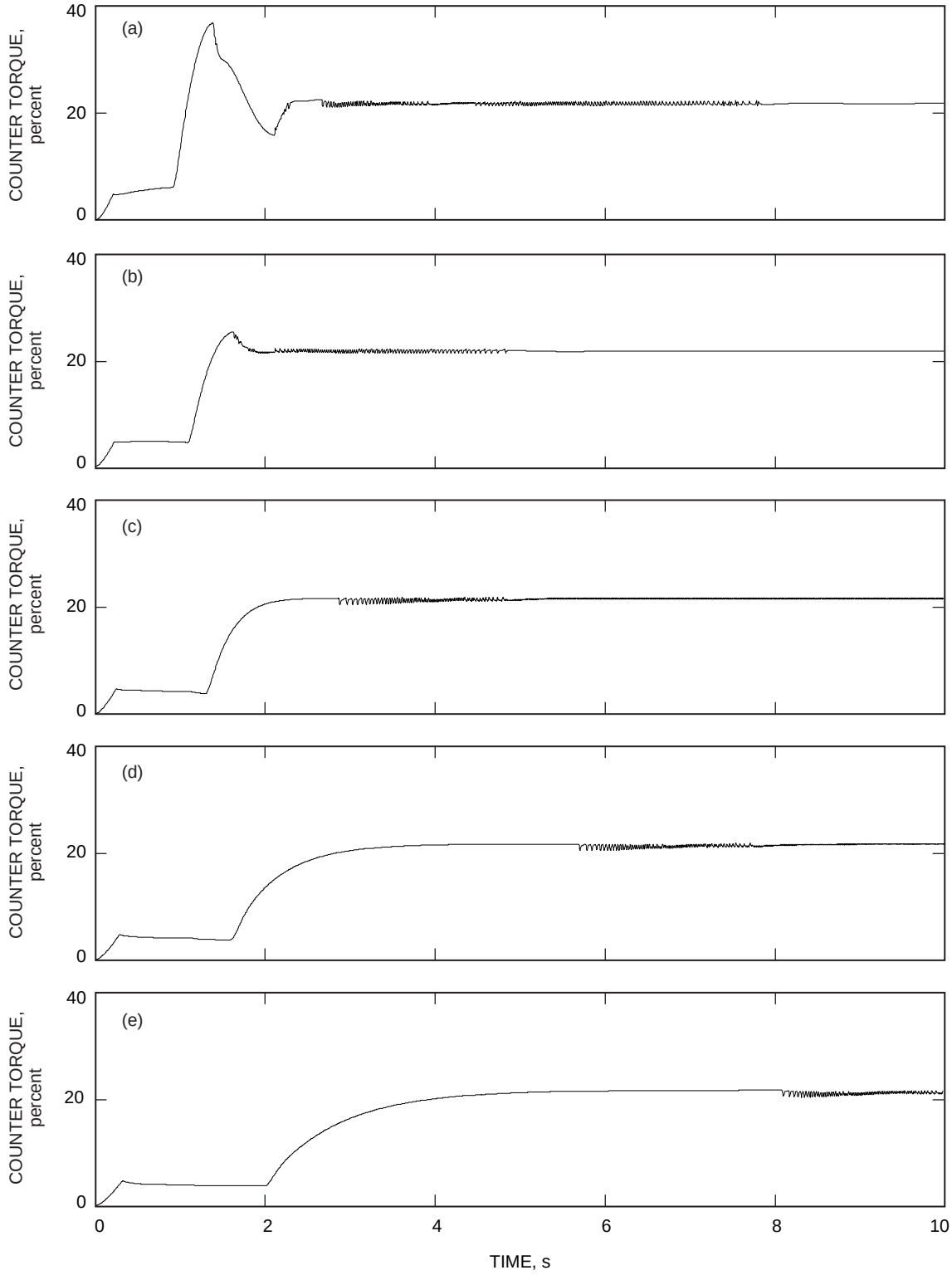

Fig. 22. Counter-torque dynamics for k_{ctfr} = 3.3 and for τ_6 of (a) 0.73 s, (b) 0.20 s, (c) 0.1125 s, (d) 0.073 s, and (e) 0.05 s.

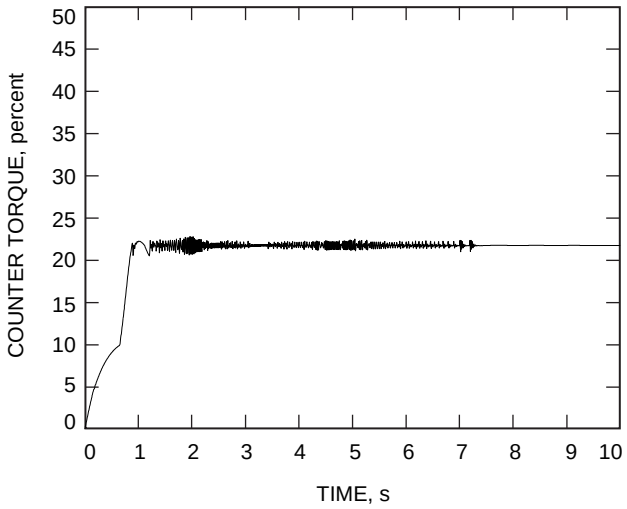

Fig. 23. Counter-torque dynamics for k_{ctfr} = 48.67 and τ_6 = 0.1125 s.